nature neuroscience

Neural substrate of dynamic Bayesian inference in the cerebral cortex

Akihiro Funamizu[1,2], Bernd Kuhn[2] & Kenji Doya[1]

Dynamic Bayesian inference allows a system to infer the environmental state under conditions of limited sensory observation. Using a goal-reaching task, we found that posterior parietal cortex (PPC) and adjacent posteromedial cortex (PM) implemented the two fundamental features of dynamic Bayesian inference: prediction of hidden states using an internal state transition model and updating the prediction with new sensory evidence. We optically imaged the activity of neurons in mouse PPC and PM layers 2, 3 and 5 in an acoustic virtual-reality system. As mice approached a reward site, anticipatory licking increased even when sound cues were intermittently presented; this was disturbed by PPC silencing. Probabilistic population decoding revealed that neurons in PPC and PM represented goal distances during sound omission (prediction), particularly in PPC layers 3 and 5, and prediction improved with the observation of cue sounds (updating). Our results illustrate how cerebral cortex realizes mental simulation using an action-dependent dynamic model.

Animals have to act despite limited sensory information because of factors such as interfering background noise or occluded vision. Thus, the ability to estimate the current state of the outside world from a sequence of sensory observations and their own actions is essential. This process is optimally realized by dynamic Bayesian inference, such as a Kalman filter[1], which predicts the state with an internal state transition model and updates the prediction with new sensory inputs. For example, when a mouse navigates in darkness, it must keep track of the location of its destination based on both its movement (prediction) and sensory signals such as calls from its nest mate (updating). We hypothesized that dynamic Bayesian inference is implemented in cerebral neocortex and investigated the plausibility of this idea using two-photon microscopy[2].

Most areas of the cerebral neocortex receive ascending sensory inputs (feedforward streams) and descending inputs (feedback streams) from the thalamus and other cortical areas[3]. Previous studies have shown that feedback streams are essential for self-motion perception, consciousness and attention[4,5], suggesting that the neocortex integrates internal state prediction on the basis of its own actions and ascending sensory signals. In addition, there have been proposals of cortical implementation of Bayesian inference using probabilistic population code[6]. A recent proposal further advocated implementation of dynamic Bayesian inference by spiking population codes[7]. In the 'canonical microcircuit' of the neocortex[3,8], feedforward signals project mainly to layer 4 and are then forwarded to layers 2/3 and 5. Pyramidal neurons in layers 2/3 and 5 receive feedback signals from their apical dendrites in layer 1 and feedforward and feedback signals merge in these neurons. Feedback signals (for example, motor activity) are stronger in deeper layers of sensory cortices[9,10]. These anatomical connections and their activity lead to the hypothesis that dynamic Bayesian inference is implemented in pyramidal neurons of layers 2, 3 and 5, with increasing action dependence in deeper layers.

To test this hypothesis, we trained mice to perform an auditory virtual navigation task and imaged neuronal activity in layers 2, 3 and 5 of the PPC and the PM located posterior to PPC[11–13]. The task required mice to approach a water reward site (goal) by estimating the distance on the basis of sound cues and their own locomotion. PPC is involved in spatial navigation by representing route maps, head directions, turning locations and locomotory accelerations with egocentric and allocentric representations[14–17]. PPC lesions disrupt navigation on the basis of self-motion information (path integration)[18,19]. PM also represents egocentric and allocentric reference frames[20]. Both PPC and PM receive inputs from auditory cortex and secondary motor cortex (M2)[21,22], but PM receives fewer feedback projections from M2 than PPC[13,23,24]. If feedback signals are important for internal state prediction based on an animal's own actions, association cortex (PPC) should show a more reliable neural implementation of dynamic Bayesian inference than the sensory cortex (PM).

We found that mice increased anticipatory licking as they approached the goal, even when sound cues were omitted, indicating that they were performing action-dependent state estimation, and that silencing of PPC by muscimol disturbed this behavior. Using probabilistic population decoding, we observed that neurons in all layers in PPC, and slightly less in PM, implemented the two fundamental features of dynamic Bayesian inference: prediction and updating. Population activity predicted the goal distance even without sounds (prediction). The uncertainty of prediction decreased with sound inputs (updating).

[1]Neural Computation Unit, Okinawa Institute of Science and Technology Graduate University, Tancha, Onna-son, Kunigami, Okinawa, Japan. [2]Optical Neuroimaging Unit, Okinawa Institute of Science and Technology Graduate University, Tancha, Onna-son, Kunigami, Okinawa, Japan. Correspondence should be addressed to K.D. (doya@oist.jp).

Received 18 March; accepted 8 August; published online 19 September 2016; doi:10.1038/nn.4390

RESULTS

Licking indicates action-dependent distance estimation

Mice were trained to perform an auditory virtual navigation task in complete darkness (Online Methods and **Fig. 1a**). Similar to a virtual-reality system with visual stimuli[25,26], navigation without vision would be a natural behavior for a burrowing and diurnal or nocturnal animal. In each trial, a sound with mixed harmonics (2–32 kHz) was presented from the virtual sound source placed at a random distance from the start position. The virtual sound source had an intensity of 100 dB SPL (sound pressure level with respect to 20 μPa) at 25-cm in virtual distance. Intensity decreased by 6 dB SPL when the apparent distance between the sound source and the mouse doubled. The virtual direction of the sound source was emulated by changing sound-generating speakers according to the mouse's locomotion on the treadmill. When the mouse passed the sound source and licked the spout, it got a water reward. The task was presented with three conditions: a continuous condition, in which sound cues were presented continuously, and two intermittent conditions, in which sounds were presented intermittently. No-sound zones in intermittent 1 or 2 conditions were alternately allocated and goal distances were randomized (**Fig. 1b**) such that mice could not predict goal distance simply from the presence or absence of auditory cues.

Mice increased licking frequency as they approached the goal (r = 0.798, $P = 2.11 \times 10^{-34}$; **Fig. 1b**; 94 sessions of 8 mice: r = 0.258 to 0.822, P = 0.00229 to 9.05×10^{-38}), indicating that mice predicted that a reward would be given at the goal. In intermittent conditions, anticipatory licking increased even when the sound was omitted (one-sided Wilcoxon signed-rank test, $P = 4.87 \times 10^{-8}$ to 1.22×10^{-15}; **Fig. 1c**).

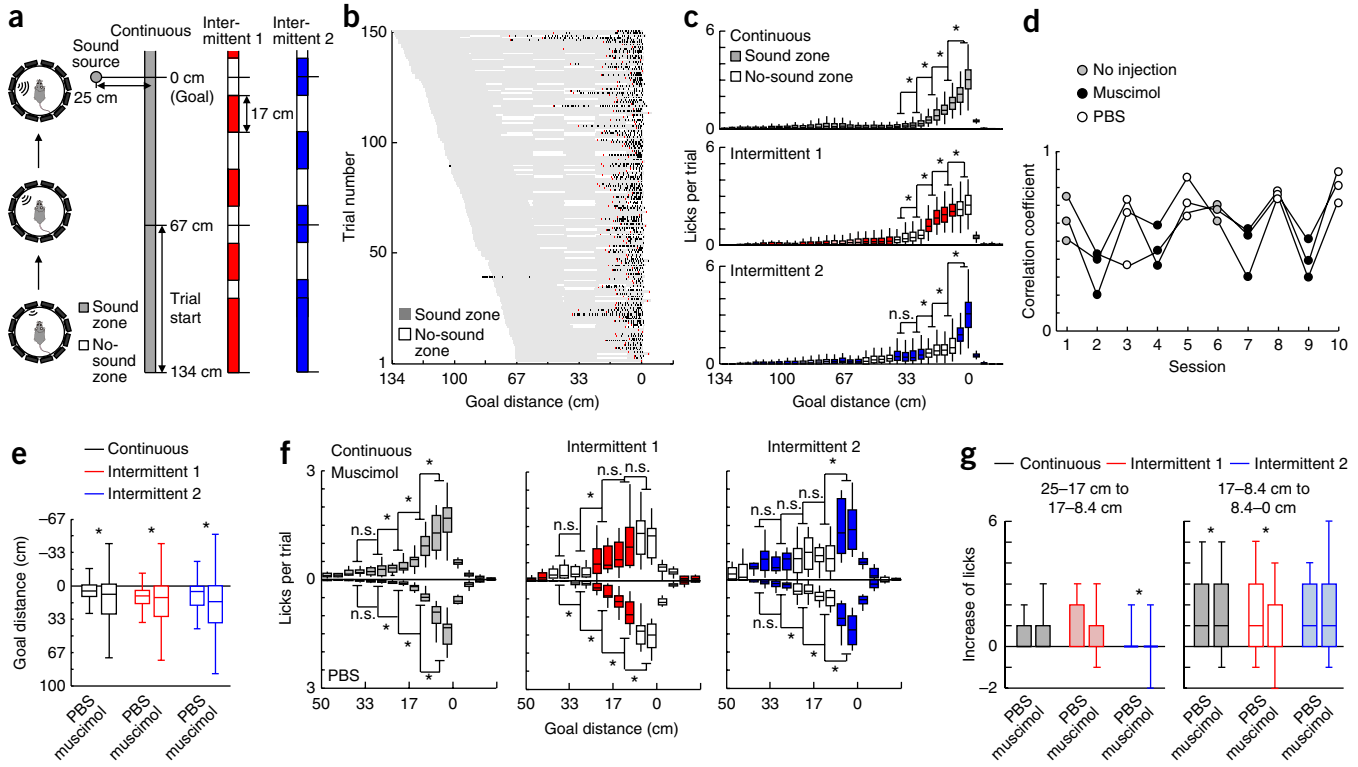

Figure 1 Auditory virtual navigation task. (**a**) Sketch showing the setup, with speakers and the three randomly presented virtual conditions starting from 134 cm. In intermittent conditions, auditory cues were always presented in the first 33 cm from start. (**b**) Licking behavior in one session (first licks red, others black). (**c**) Average licking behavior (94 sessions, 8 mice; central mark in box, median; edge of box, 25th and 75th percentiles; whiskers, most extreme data points not considered outliers (beyond 1.5× the inter-quartile range), $^*P < 10^{-7}$ in one-sided Wilcoxon signed-rank test; continuous: $P = 5.64 \times 10^{-13}$, 4.45×10^{-17}, 1.94×10^{-17}, 1.94×10^{-17}, z = 7.11, 8.32, 8.42, 8.42; intermittent 1: $P = 1.22 \times 10^{-15}$, 2.34×10^{-17}, 4.51×10^{-14}, 4.87×10^{-8}, z = 7.91, 8.39, 7.45, 5.33; intermittent 2: P = 0.0160, 2.61×10^{-8}, 3.08×10^{-10}, 2.00×10^{-17}, z = 2.14, 5.44, 6.19, 8.41). Anticipatory licking increased during the absence of auditory cues, indicating action-dependent goal-distance estimation by mice. (**d**) Correlation between the start-to-lick distance and start-to-goal distance after muscimol injection. Muscimol or phosphate-buffered saline (PBS) were alternately injected into the PPC of three mice in each session. Correlation coefficients decreased after muscimol injection, indicating that silencing of PPC made lick initiation more variable (Mann-Whitney U test, $P = 3.08 \times 10^{-4}$, z = 3.61). (**e**) Distance between the first lick and the goal. Variance of the distance was compared between PBS and muscimol-injected trials (continuous, n = 1,407, 1,188; intermittent 1, n = 293, 240; intermittent 2, n = 259, 230) (box plot as in **c**, $^*P < 10^{-14}$ in Ansari-Bradley test; continuous: $P = 4.35 \times 10^{-56}$, w = 15.8; intermittent 1, $P = 2.70 \times 10^{-15}$, w = 7.90; intermittent 2, $P = 2.53 \times 10^{-24}$, w = 10.2). (**f**) Average licking behavior after muscimol or PBS injection (12 sessions, 3 mice, box plot as in **c**, $^*P < 0.01$ in one-sided Wilcoxon signed-rank test; muscimol: continuous, P = 0.0615, 0.00684, 2.44×10^{-4}, 2.44×10^{-4}, w = 51, 60, 78, 78; intermittent 1, P = 0.238, 0.00342, 0.0320, 0.0212, w = 35, 62, 63, 65; intermittent 2, P = 0.416, 0.0615, 0.485, 7.32×10^{-4}, w = 36, 51, 40, 76; PBS: continuous, P = 0.0161, 0.00244, 2.44×10^{-4}, 2.44×10^{-4}, w = 57, 73, 78, 78; intermittent 1, P = 0.00195, 0.00293, 2.44×10^{-4}, 2.44×10^{-4}, w = 54, 53, 78, 78; intermittent 2, P = 0.0166, 0.00464, 0.00147, 2.44×10^{-4}, w = 66, 71, 64, 78). Increase of licking during no-sound zones was disrupted after muscimol injection, indicating that PPC was involved in action-dependent, goal-distance estimation. (**g**) Comparison of increase of lick counts in two adjacent distance bins in PBS and muscimol-injected trials (continuous, n = 1,407, 1,188; intermittent 1, n = 293, 240; intermittent 2, n = 259, 230) (central mark in box, median; edge of box, 25th and 75th percentiles; whiskers, 10th and 90th percentiles; $^*P < 0.01$ in Mann-Whitney U test; 25–17 cm to 17–8.4 cm, P = 0.116, 0.0149, 0.00761, z = 1.57, 2.43, 2.67; 17–8.4 cm to 8.4–0 cm, $P = 3.86 \times 10^{-8}$, 4.84×10^{-6}, 0.652, z = 5.50, 4.57, 0.451). Colored and white bars show the licking during sound and no-sound zones, respectively.

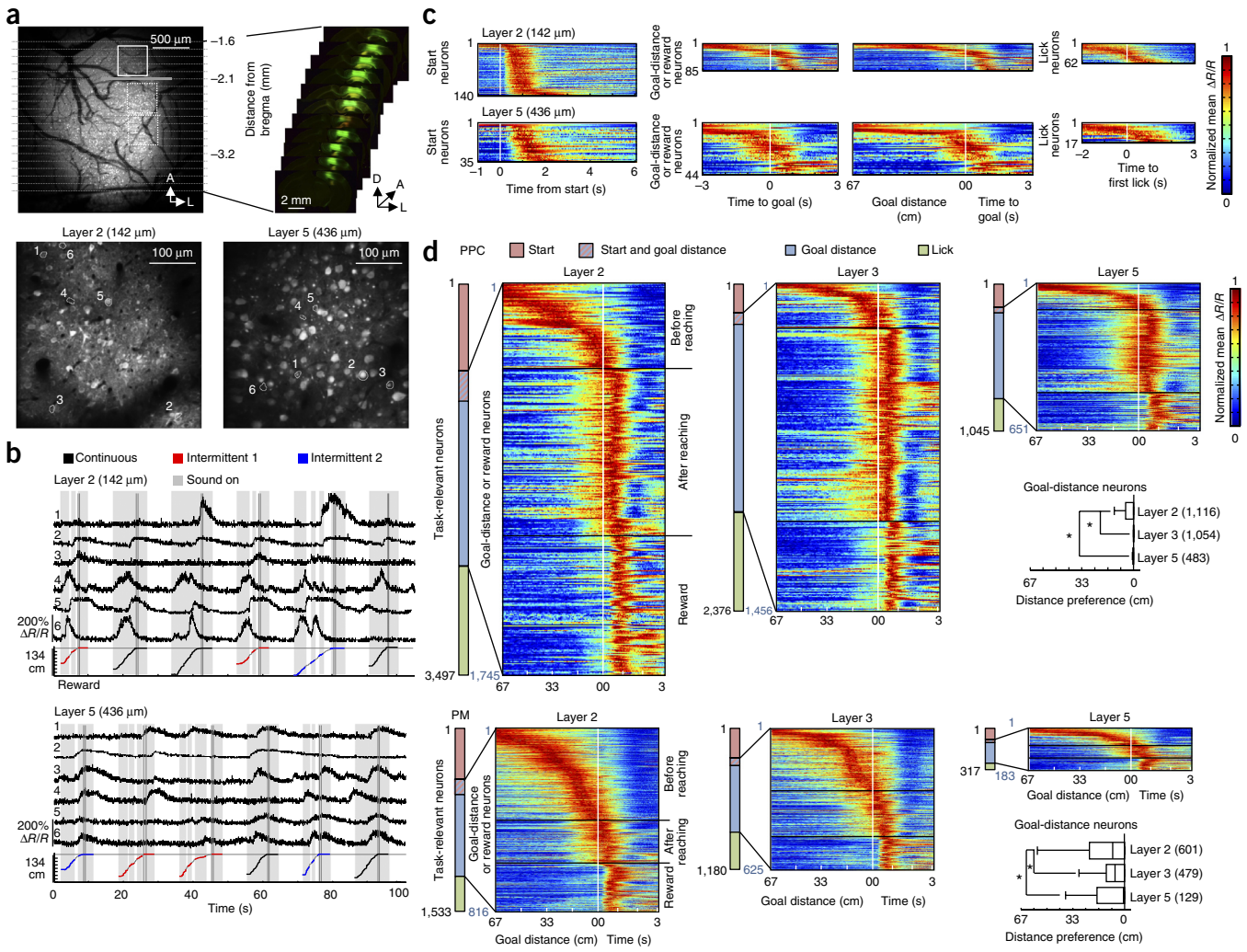

Figure 2 Two-photon (2P) imaging of neuronal activity in PPC and PM during the task. (**a**) Imaging locations in an overview image (thick line indicates border between PPC (anterior) and PM (posterior)), post mortem brain slices and *in vivo* 2P imaging with cellular resolutions at the closed square position. (**b**) Activity traces of PPC neurons marked in **a** and corresponding locomotion in six example trials. Colors at the bottom show trial conditions. Sound zones are shown in gray. (**c**) Task-relevant neurons in **a**. Goal-distance and reward neurons are aligned by time and distance-to-goal. Neural activity after reaching the goal (0 cm distance) is shown as time aligned, as the goal-distance sound was terminated after the reward delivery. Neural activity of all trials was averaged, normalized, and sorted by peak times. (**d**) Goal-distance and reward neurons of all sessions ($n = 94$). Bars indicate the proportion of neurons representing each variable. Although similar numbers of neurons were analyzed (20,338 in PPC and 20,693 in PM), PPC had more task-relevant neurons and after-reaching neurons than PM. Insets, distribution of peaks of distance coding in goal-distance neurons. Parentheses show the number of goal-distance neurons (central mark in box, median; edge of box, 25th and 75th percentiles; whiskers, most extreme data points not considered outliers (beyond 1.5× the inter-quartile range), $^*P < 0.01$ in Mann-Whitney *U* test; PPC, comparison of layer 2/3, 2/5, 3/5, $P = 2.25 \times 10^{-16}$, 1.07×10^{-6}, 0.154, $z = 8.21$, 4.88, 1.43; PM, $P = 0.00147$, 0.00319, 0.252, $z = 3.18$, 2.95, 1.15). Neurons in layers 3 and 5 represented distances closer to the goal than neurons in layer 2.

During sound omissions, increased licking depended on the locomotion speed (**Supplementary Fig. 1**), suggesting that mice estimated the goal distance (or the virtual sound-source position) on the basis of their own actions using an internal state transition model, and not merely on the basis of the time from the offset of sound.

To investigate whether PPC is involved in action-dependent distance estimation, we silenced PPC using the GABA-A receptor agonist muscimol[25]. Silencing of PPC made the lick initiations more variable (Mann-Whitney *U*-test, $P = 3.08 \times 10^{-4}$; **Fig. 1d**; Ansari-Bradley test, $P = 2.70 \times 10^{-15}$ to 4.35×10^{-56}; **Fig. 1e** and **Supplementary Fig. 2**). The effect of PPC silencing was most prominent in intermittent conditions, with no increase in licking in no-sound zones (one-sided Wilcoxon signed-rank test, $P = 0.485$ to 0.0212; **Fig. 1f**; Mann-Whitney *U*-test, $P = 0.00761$ and 4.84×10^{-6}; **Fig. 1g**). In addition, PPC silencing delayed licking for reward acquisition in the no-sound zone in intermittent 1 condition (**Supplementary Fig. 2d**). These results indicate that PPC is involved in goal distance estimation, particularly during action-dependent state prediction.

Goal-distance representation in PPC and PM

We optically imaged neuronal activity of layers 2, 3 and 5 of PPC and PM with the genetically encoded calcium indicator GCaMP6f (Online Methods and **Fig. 2a**). The field of view was 400 × 400 μm. Recorded regions, determined on the basis of the blood-vessel pattern, and the relative position of the fluorescent area and subcortical structures[11], were mainly lateral parietal association cortex (LPtA) and secondary

visual cortex mediolateral area (V2ML) for PPC and PM, respectively (**Supplementary Fig. 3**). These regions correspond to AM and PM of previous publications[12,13]. In total, we imaged the activity of 41,031 neurons in 94 sessions (PPC: 8,371, 7,108 and 4,859 neurons from 17, 15 and 14 sessions in layers 2, 3 and 5, respectively; PM: 7,788, 7,005 and 5,900 neurons from 16, 15 and 17 sessions, respectively).

Although PPC and PM are sometimes classified as higher visual areas[12,13], we found robust sound responses (**Supplementary Fig. 4**). Some neurons increased activity after sound presentations, consistent with a recent study[22]. On average, PM had more sound-responsive neurons than PPC in layer 3 (PPC, 1.48%, PM, 4.78%; Mann-Whitney *U* test, $P = 0.0402$).

PPC neurons increased activity during different phases of the task, such as approaching or after reaching the goal (**Fig. 2b**). We investigated task-relevant neurons, which showed a significant increase in activity during trials (one-sided one-sample *t*-test, $P < 10^{-10}$) (**Fig. 2c**). We classified neurons that changed activity while approaching the goal as goal-distance neurons and further subdivided them into before-reaching and after-reaching neurons, depending on when their activity peaked. Other neurons increased their activity with the reward (reward neurons), at the start of trials (start neurons) and during initiation of licking (lick neurons). Task-irrelevant neurons increased activity during inter-trial intervals, only in a small number of trials, at random timing or showed only small fluorescence changes (**Supplementary Fig. 5**).

Among active neurons (99.6% of all neurons; **Supplementary Table 1**), the proportions of task-relevant neurons in layers 2, 3 and 5 were 41.3, 33.8 and 20.0% in PPC, and 19.6, 16.7 and 5.70% in PM, indicating that more neurons were recruited to the task in PPC than PM (Mann-Whitney *U* test, $P = 3.38 \times 10^{-4}$, 0.0202 and 2.81×10^{-4}, $z = 3.58$, 2.32 and 3.63 in layers 2, 3 and 5, respectively). PPC had more goal-distance neurons than PM in all layers (Mann-Whitney *U* test, $P = 0.00415$, 0.0152 and 4.98×10^{-4}, $z = 2.87$, 2.43 and 3.48, respectively; **Fig. 2d**). PPC had more after-reaching neurons than before-reaching neurons (Wilcoxon signed-rank test, $P = 0.0319$, 0.00568 and 0.0176, $z = 2.15$, $w = 13.5$ and 9.5), whereas PM had the opposite tendency ($P = 0.00771$, 0.287 and 0.427, $z = 2.66$, $w = 70$ and 57.5). Thus, goal-distance neurons in PPC mainly represented the distance near the goal, whereas PM had relatively distributed representations. Moreover, in both areas, goal-distance neurons in layers 3 and 5 were more tuned to the distance near the goal than those in layer 2 (Mann-Whitney *U* test, $P = 0.00319$ to 2.25×10^{-16}).

We then tested whether goal-distance neurons in PPC and PM best represented the goal distance, goal time or other variables (that is, licking frequency or locomotion speed). In our task, locomotion speed of mice varied across trials (**Fig. 3a**) so that the distance and the time to reach the goal were separable. For example, we aligned the activity of an after-reaching neuron with goal time or goal distance (**Fig. 3a**). The distance-aligned activity had similar traces, irrespective of locomotion speeds, indicating that this neuron encoded goal distance rather than time.

To quantitatively analyze representations of goal-distance neurons, we conducted a regression analysis of neural activity with multiple variables (equation (2) and **Fig. 3b**). The regression analysis tested whether activity was correlated with distance or time to reach the goal, and tested whether the activity was correlated with licking frequency and locomotion speed. More neurons represented the goal distance than the time to goal in PPC and PM (Wilcoxon signed-rank test, $P = 0.00348$ to 4.33×10^{-4}). Activities of some neurons were also modulated by locomotion speed and licking frequency, indicating that neurons represent more than just goal distance, consistent with

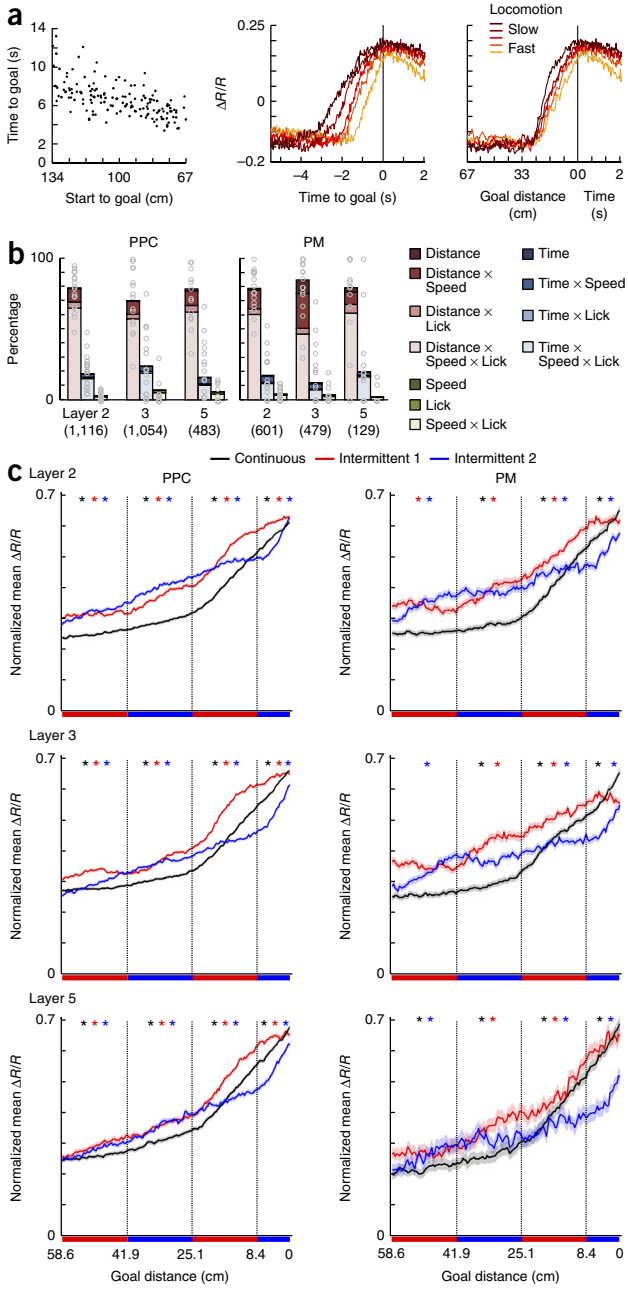

Figure 3 Action-dependent distance representation. (**a**) Distinction of goal-time- and goal-distance-encoding neurons. Distribution of time-to-goal and start-to-goal-distance pairs in one session (left). Activity traces of one neuron grouped and averaged by locomotion speed, aligned with time (middle) and distance to goal (right) indicate distance encoding. (**b**) Regression analysis of all goal-distance neurons (equation (2)). Parentheses show the number of goal-distance neurons. PPC and PM neurons represented the goal distance rather than the time to reach goal (Wilcoxon signed-rank test, PPC layers 2, 3, 5, $P = 4.33 \times 10^{-4}$, 0.00348, 0.00146, $w = 136$, 108.5, 87; PM, $P = 5.29 \times 10^{-4}$, 0.00153, 8.54×10^{-4}, $w = 135$, 112, 101). (**c**) Averaged normalized activity traces of all after-reaching neurons. Sound zones in intermittent 1 and intermittent 2 conditions are indicated by red and blue bars, respectively. Linear regression analysis tested whether the slope of activity in each neuron was significantly positive during sound and no-sound zones (equation (5)) (mean ± s.e.m., $^*P < 0.01$ in Wilcoxon signed-rank test, $P = 0.483$ to 0, $z = 0.702$ to 25.0). Number of after-reaching neurons in layers 2, 3, 5 was 744, 854, 367 in PPC and 193, 204, 54 in PM. After-reaching neurons in PPC increased the activity even without sound.

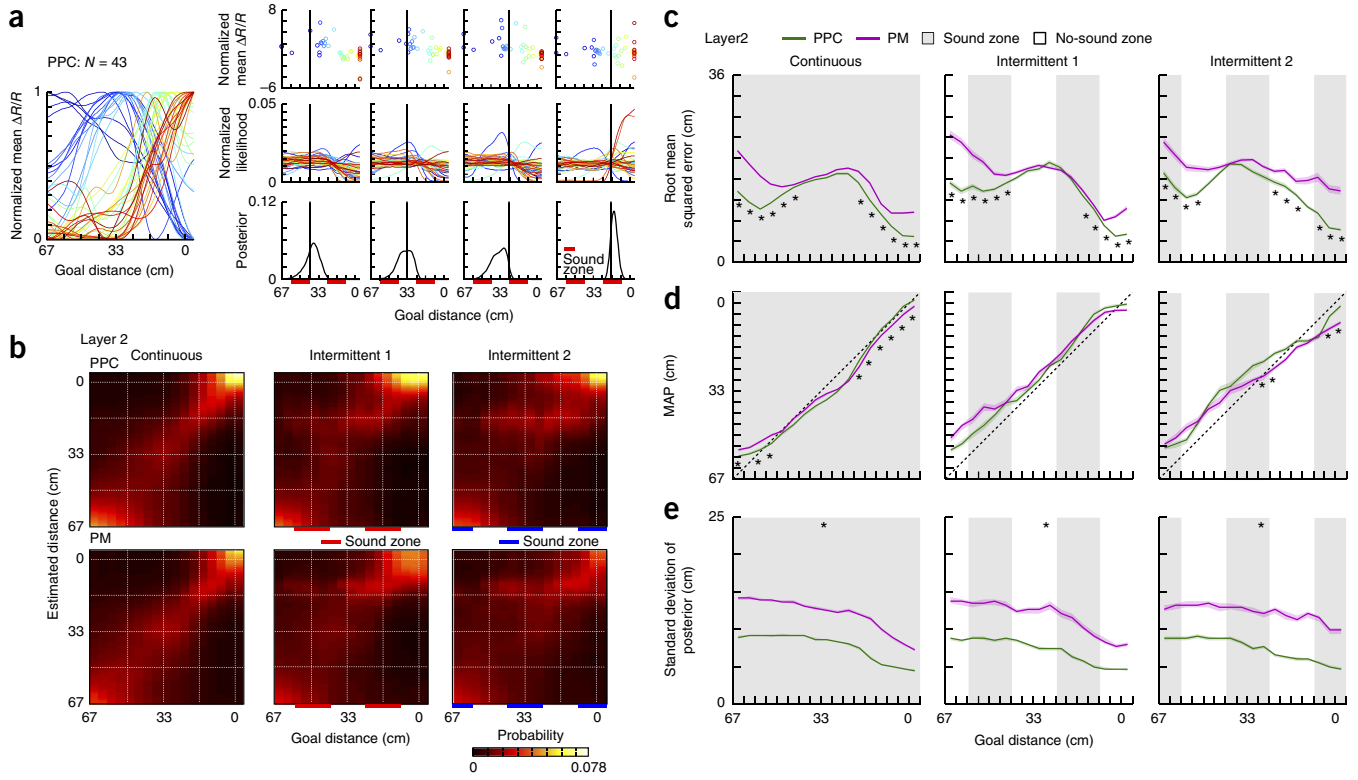

Figure 4 Probabilistic decoding. (**a**) Procedure. Left, normalized distance tuning curves of layer 2 goal-distance neurons shown in **Figure 2a**. Right, four examples of posterior calculation with the mouse's actual position shown with a vertical line. Instantaneous activities of goal-distance neurons are plotted at their peak-activity distances (top). Activity was scaled based on distance tuning curves to give likelihoods of distance for all goal-distance neurons (middle). Product of all likelihoods and a flat, non-informative prior gave the posterior probability of goal distance (bottom). (**b**) Average goal-distance distributions estimated from layer 2 neurons in PPC and PM under actual goal distances from 67 to 0 cm. (**c**) Decoding performance from layer 2 neurons in PPC and PM. Root mean squared error was the expected squared deviation of the estimated and actual goal distances (median ± robust standard error, $*P < 0.01$ in Mann-Whitney U test; continuous, $P = 0.893$ to 0, $z = 0.134$ to 17.1; intermittent 1, $P = 0.748$ to 0, $z = 0.322$ to 8.42; intermittent 2, $P = 0.738$ to 0, $z = 0.334$ to 8.55) (number of trials in PPC and PM; continuous, $n = 1,785$, 1,721; intermittent 1, $n = 398$, 362; intermittent 2, $n = 367$, 317). (**d**) MAP is the mode of estimated distance (continuous, $P = 0.594$ to 2.47×10^{-11}, $z = 0.533$ to 6.68; intermittent 1, $P = 0.893$ to 0.0279, $z = 0.135$ to 2.20; intermittent 2, $P = 0.961$ to 8.81×10^{-6}, $z = 0.0485$ to 4.44). (**e**) s.d. of posterior is the spread of estimation from the MAP estimate ($P = 1.09 \times 10^{-12}$ to 0, $z = 7.12$ to 22.9). PPC neurons encoded the goal distance more accurately with higher certainty than PM neurons.

previous findings[15,20]. We also verified that activities were correlated with goal distance rather than sound intensity or the distance assumed to be constant during no-sound zones (**Supplementary Fig. 6**). Fitted coefficients for goal-distance representation revealed that the distance tuning curves of neurons were similar between PPC and PM (Online Methods; Mann-Whitney U test, $P = 0.268$ to 0.106, $z = 1.11$ to 1.62).

PPC represents goal distance estimated from action

Given that licking behavior indicates action-dependent distance estimation (**Fig. 1**), neural representation of goal distance may also change during the approach, even in the absence of sound inputs. We analyzed the activity of after-reaching neurons and found that this was true in PPC and partially so in PM. Activity in the continuous condition gradually increased in both PPC and PM as mice approached the goal (Wilcoxon signed-rank test, $P = 0.00507$ to 0, $z = 2.80$ to 25.0; **Fig. 3c**, and **Supplementary Figs. 7** and **8a**). In intermittent conditions, increased activity was observed with and without sound inputs in all PPC layers (sound zones: $P = 1.37 \times 10^{-4}$ to 0, $z = 3.81$ to 23.2; no-sound zones: $P = 1.19 \times 10^{-6}$ to 0, $z = 4.86$ to 17.9), although the slopes of activity without sound were lower than those with sound (**Supplementary Fig. 8b**). Positive slopes of activity were also observed in PM in some no-sound zones ($P = 2.40 \times 10^{-4}$ to 0, $z = 3.67$ to 9.59), but the slopes were equal to or lower than those in PPC (**Supplementary Fig. 8c**). Thus, a subset of neurons in PPC and PM represent goal distance based on locomotion corresponding to licking behavior.

We also investigated whether distance representation in the continuous condition was preserved in intermittent conditions (**Supplementary Fig. 9**). PPC neurons preserved the distance representation, especially near the goal, significantly more than neurons in PM (Mann-Whitney U test, $P = 0.0429$ to 6.82×10^{-14}, $z = 2.02$ to 7.49), suggesting a robust action-dependent distance representation.

Distance prediction with dynamic Bayesian inference

To test whether the population of neurons in PPC and PM represents the goal distance as expected in dynamic Bayesian inference, we conducted a probabilistic decoding analysis. The decoder was based on probabilistic population coding[27–29], which assumed that the probability distribution of the goal distance was represented by the population activity of neurons (**Fig. 4a**). We constructed a goal distance decoder from the activity of goal-distance neurons in each field of view using data in continuous condition for training. We first characterized the distance-tuning curve of each neuron, and then calculated the likelihood of goal distance from neural activity at each moment. The likelihood from each neuron was then multiplied with a flat prior distribution to produce the posterior distribution. The probabilistic decoder provided not only the most probable distance

(maximum a posterior, MAP), but also the uncertainty (s.d. of posterior distribution). In the example trial (**Fig. 4a**), MAP advanced with and without sound inputs. Although uncertainty (width of posterior distribution) increased during no-sound zones, it decreased after sound presentations near the goal.

We compared estimated goal distances between PPC and PM (layer 2; **Fig. 4b**; layers 3 and 5; **Supplementary Fig. 10**). Both areas estimated the goal distances reliably above chance level (Wilcoxon signed rank test, $P = 0$, $z = 181$ to 439), and the estimation in PPC had significantly less deviation from the actual distance than in PM (Mann-Whitney

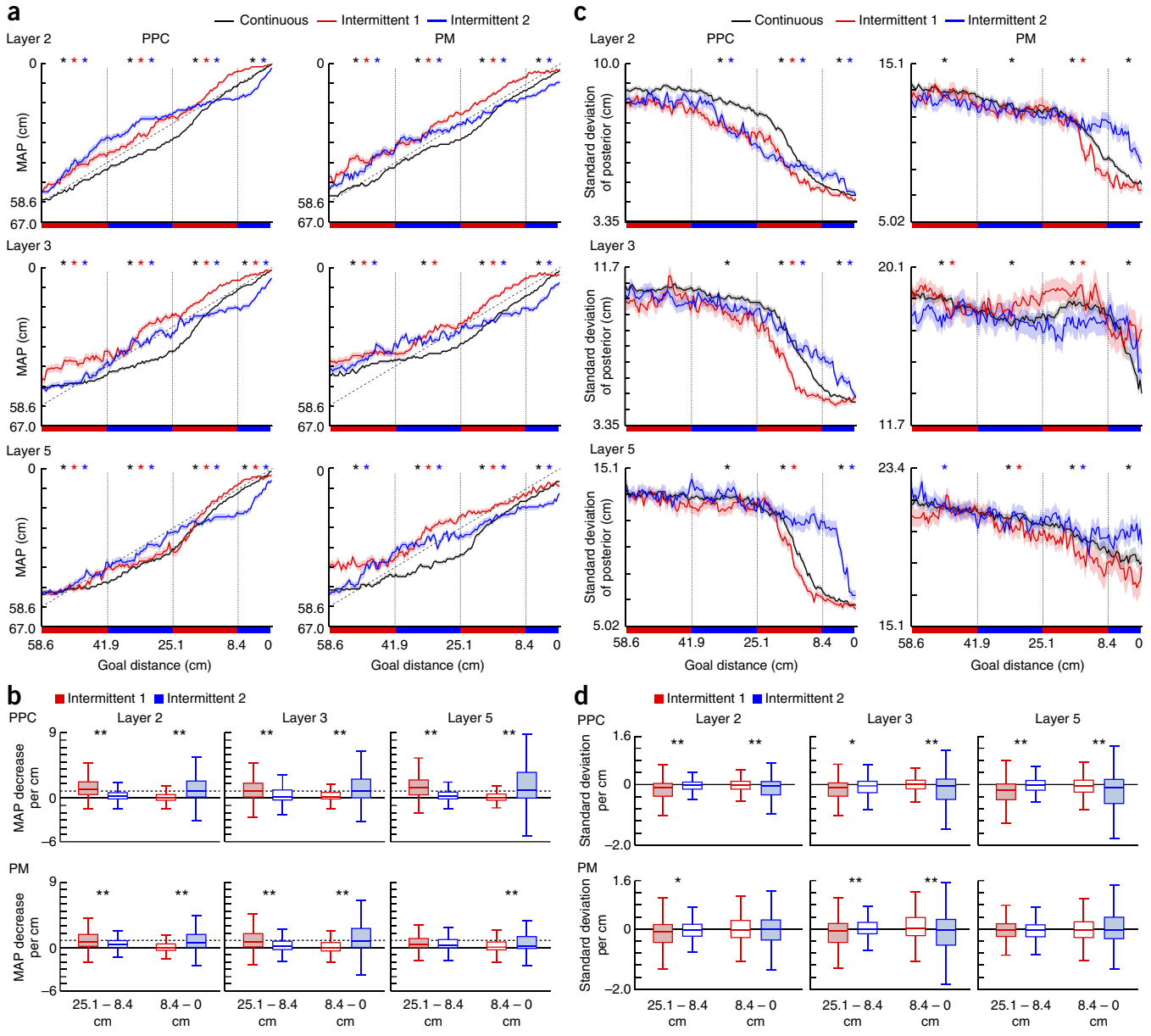

Figure 5 Goal-distance neurons estimate distance with dynamic Bayesian inference. (**a**) Estimated distance. Linear regression analysis investigated the slope of the estimated distance (MAP) in each trial during sound and no-sound zones (equation (10)). MAP decreased with and without sound in layers 3 and 5 of PPC (median ± robust s.e., $*P < 0.01$ in Wilcoxon signed-rank test, $P = 0.218$ to 0, $z = 1.23$ to 34.1) (number of trials in continuous, intermittent 1 and intermittent 2 conditions: PPC layer 2, $n = 1{,}785$, 398, 367; layer 3, $n = 1{,}585$, 331, 334; layer 5, $n = 1{,}445$, 347, 308; PM layer 2, $n = 1{,}721$, 362, 317; layer 3, $n = 1{,}571$, 348, 331; layer 5, $n = 1{,}438$, 331, 331). (**b**) Comparison of estimated distance during sound and no-sound zones. Slopes of MAP were compared between intermittent 1 and intermittent 2 conditions (central mark in box, median; edge of box, 25th and 75th percentiles; whiskers, most extreme data points not considered outliers (beyond 1.5× the inter-quartile range), $*P < 0.05$, $**P < 0.01$ in Mann-Whitney U test; PPC layer 2, $P = 0$, 0, $z = 12.5$, 11.0; layer 3, $P = 5.14 \times 10^{-12}$, 1.06×10^{-13}, $z = 6.90$, 7.43; layer 5, $P = 0$, 0, $z = 10.8$, 8.84; PM layer 2, $P = 7.36 \times 10^{-8}$, 5.88×10^{-15}, $z = 5.38$, 7.81; layer 3, $P = 2.89 \times 10^{-14}$, 3.66×10^{-15}, $z = 7.60$, 7.87; layer 5, $P = 0.241$, 0.00129, $z = 1.17$, 3.22). Colored and white bars show the slopes with and without sound, respectively. (**c**) Uncertainty of distance estimation. Linear regression analysis investigated the slope of uncertainty (s.d. of posterior). Data presentation as in **a** (Wilcoxon signed-rank test, $P = 0.892$ to 0, $z = 0.135$ to 19.5). Uncertainty decreased during sound presentations in PPC between 8.4 cm and 0 cm. (**d**) Comparison of uncertainty during sound and no-sound zones. Data presentation as in **b** (Mann-Whitney U test; PPC layer 2, $P = 9.12 \times 10^{-8}$, 9.92×10^{-4}, $z = 5.34$, 3.29; layer 3, $P = 0.0153$, 0.00419, $z = 2.42$, 2.86; layer 5, $P = 6.92 \times 10^{-11}$, 0.00285, $z = 6.52$, 2.98; PM layer 2, $P = 0.0389$, 0.591, $z = 2.06$, 0.537; layer 3, $P = 6.34 \times 10^{-4}$, 0.00396, $z = 3.42$, 2.88; layer 5, $P = 0.611$, 0.406, $z = 0.508$, 0.831).

U-test in layer 2, $P = 0.00765$ to 0, $z = 2.67$ to 17.1) (**Fig. 4c** and **Supplementary Fig. 10**). Decoding errors decreased with sound and increased without sound (Mann-Whitney *U* test, $P = 0.00295$ to 1.56×10^{-6}, $z = 2.97$ to 4.80; **Supplementary Fig. 11**), suggesting that sound observations calibrate the distance estimation of neurons. PPC and PM had similar MAP estimates, but the estimations near the goal were better in PPC than in PM ($P = 0.00549$ to 2.47×10^{-11}, $z = 2.78$ to 6.68; **Fig. 4d**). In addition, uncertainty of distance estimation was significantly less in PPC than PM ($P = 1.09 \times 10^{-12}$ to 0, $z = 7.12$ to 22.9; **Fig. 4e**), possibly because the number of recruited neurons for the decoder was large in PPC (average number of goal-distance neurons in layers 2, 3 and 5; PPC, 65.6, 70.3 and 34.5; PM, 37.6, 31.9 and 7.59) or because PPC receives and integrates additional inputs. Thus, PPC and PM estimate the distance, but PPC is more precise than PM.

We then focused on how estimated distances change during the absence of sound inputs (**Fig. 5** and **Supplementary Fig. 12**). In the continuous condition, MAPs followed the actual distances in all layers of PPC and PM (Wilcoxon signed-rank test, $P = 9.56 \times 10^{-14}$ to 0, $z = 7.45$ to 34.1; **Fig. 5a**). In intermittent conditions, MAPs decreased with and without sound inputs in most distance zones, and especially in all zones in PPC layers 3 and 5 (sound zones: $P = 0.00293$ to 0, $z = 2.98$ to 14.7; no-sound zones: $P = 6.59 \times 10^{-4}$ to 0, $z = 3.41$ to 8.56). Slopes of MAPs without sound were lower than those with sound (Mann-Whitney *U* test, $P = 5.14 \times 10^{-12}$ to 0; **Fig. 5b**). In the intermittent 1 condition, the decrease of MAPs in PPC layer 3 was significantly steeper than that in layer 2 without sound between 8.4 and 0 cm (Mann-Whitney *U* test, $P = 0.00685$, $z = 2.70$), whereas the s.d. of distance estimation showed no significant difference ($P = 0.247$, $z = 1.16$), suggesting that there were some differences in prediction among layers. The decrease of MAPs was rapid when mice moved fast during no-sound zones (**Supplementary Fig. 13**), suggesting that PPC and PM realize the action-dependent distance prediction. Uncertainty of estimated distance decreased with sound inputs compared with no sound in all layers of PPC between 25.8 and 0 cm ($P = 0.0153$ to 6.92×10^{-11}; **Fig. 5c**,**d**), consistent with the updating step of dynamic Bayesian inference.

DISCUSSION

Behavioral studies have suggested that the brain employs Bayesian computation during multi-modal cue integration[30], sensorimotor transformations[31] and sensory-evidence accumulations[32] by computing not just single values, but the probabilistic distribution of sensory and motor variables. Previous studies, however, addressed Bayesian computation with only non-dynamic sensory generative models[32] or action-independent state transition models[33]. To the best of our knowledge, our study represents the first optical neuroimaging experiment to directly test neural implementation of action-dependent dynamic Bayesian inference, which can be the basis for mental simulation and other cognitive operations.

It has been hypothesized that Bayesian inference is implemented in cerebral cortex, including PPC, on the basis of anatomy[34,35], function[36] and population activity[29]. In addition, dynamic Bayesian inference using internal state transition models, such as a Kalman filter, has been realized by neural network models[6,7,37,38]. In this study, animals increased anticipatory licking even during no-sound zones, and this was impaired by inactivation of PPC (**Fig. 1**), indicating that the cerebral cortex is involved in dynamic Bayesian inference. Using two-photon imaging and probabilistic neural population decoding, we provide, to the best of our knowledge, the first direct evidence that the neocortical circuit implements dynamic Bayesian inference: prediction of changing states even without sensory input and sharpening of prediction when given sensory input (**Fig. 5**).

Decoded goal distance decreased significantly in all no-sound zones in layers 3 and 5 of PPC, and in most no-sound zones in other tested locations (**Fig. 5a**). The decrease of uncertainty near the goal was significantly steeper with sound than without sound in all PPC layers (**Fig. 5d**). There were apparent decreases in uncertainty near the goal even without sound (for example, layers 2 and 3 in PPC), which could be a result of denser representation of the distance close to the goal (**Fig. 2d**). Although goal distances and presented sound intensities were correlated, neurons represented the goal distance more consistently than the sound intensity (**Supplementary Fig. 6**).

Dynamic Bayesian inference requires an action-dependent state transition model. Although both PPC and PM receive sound inputs from auditory cortex, PPC receives stronger locomotory inputs from the secondary motor cortex (M2) than PM (**Supplementary Fig. 14**)[13,23,24], which is consistent with observations of better prediction in PPC than in PM (**Fig. 4**). PPC has reciprocal connections with the hippocampus via entorhinal cortex and retrosplenial cortex. PPC also has connections with presubiculum[13], which contains grid cells[39]. These connections may enable PPC to contribute to place coding[14,23]. Feedforward sensory signals to layer 4 and feedback motor signals to layer 1 merge in pyramidal neurons layers 2, 3 and 5, with the latter through the apical dendrites[3,8]. Consistent with such commonality in anatomical connections, the difference in goal-distance coding in layers 2, 3 and 5 was more quantitative than qualitative (**Fig. 5**). Among the three layers in both areas, neurons in layers 3 and 5 of PPC most consistently showed signatures of dynamic Bayesian inference: prediction even without sensory input and updating with sensory input. The proportion of neurons with peak activity near the goal increased with depth (**Fig. 2d**), suggesting that the accuracy of goal representation increases in deeper layers.

Some previous studies have suggested distinct sensory representations between layers 2/3 and 5 in the somatosensory cortex of rat and the visual cortex of mouse[3,5,9,10]. These studies used unexpected sensory stimuli to produce mismatches between predictive sensory signals and actual sensory inputs, implying that cortical laminar structure reduces state prediction errors[35]. Further experiments and analyses of sensory mismatches may reveal a distinct laminar implementation of dynamic Bayesian inference. In addition, imaging from auditory cortex and M2, or simultaneous imaging of multiple layers in PPC with higher temporal resolution, may reveal how the sensory likelihood and an action-dependent prior are dynamically integrated.

In summary, we found that PPC and PM neurons represent essential signs of dynamic Bayesian inference: prediction by an action-dependent internal model and updating by sensory input. These features were most robust in layers 3 and 5 of PPC. This observation provides an important clue as to how dynamic Bayesian inference is implemented in the neocortical microcircuit.

METHODS

Methods, including statements of data availability and any associated accession codes and references, are available in the online version of the paper.

Note: Any Supplementary Information and Source Data files are available in the online version of the paper.

ACKNOWLEDGMENTS

We thank the GENIE Program and the Janelia Research Campus for distributing GCaMP6f. We thank S.D. Aird for editing the manuscript and K. Mori for technical assistance. This work was supported by a Grant-in-Aid for Scientific Research on Innovative Areas: Prediction and Decision Making (23120007) (K.D.), KAKENHI 26730124 (A.F.) and 15H01452 (A.F.), and internal funding from the Okinawa Institute of Science and Technology Graduate University (K.D. and

B.K.). We are grateful for generous support from the Okinawa Institute of Science and Technology Graduate University to the Neural Computation and Optical Neuroimaging Units.

AUTHOR CONTRIBUTIONS

A.F. designed the study, built the setup, collected and analyzed data, and wrote the paper. B.K. designed the study, built the setup and wrote the paper. K.D. designed the study and wrote the paper.

COMPETING FINANCIAL INTERESTS

The authors declare no competing financial interests.

1. Doya, K., Ishii, S., Pouget, A. & Rao, R.P. *Bayesian Brain: Probabilistic Approaches to Neural Coding* (MIT Press, 2007).
2. Denk, W., Strickler, J.H. & Webb, W.W. Two-photon laser scanning fluorescence microscopy. *Science* **248**, 73–76 (1990).
3. Larkum, M. A cellular mechanism for cortical associations: an organizing principle for the cerebral cortex. *Trends Neurosci.* **36**, 141–151 (2013).
4. Noudoost, B., Chang, M.H., Steinmetz, N.A. & Moore, T. Top-down control of visual attention. *Curr. Opin. Neurobiol.* **20**, 183–190 (2010).
5. Keller, G.B., Bonhoeffer, T. & Hübener, M. Sensorimotor mismatch signals in primary visual cortex of the behaving mouse. *Neuron* **74**, 809–815 (2012).
6. Beck, J.M., Latham, P.E. & Pouget, A. Marginalization in neural circuits with divisive normalization. *J. Neurosci.* **31**, 15310–15319 (2011).
7. Boerlin, M. & Denève, S. Spike-based population coding and working memory. *PLoS Comput. Biol.* **7**, e1001080 (2011).
8. Shipp, S. Structure and function of the cerebral cortex. *Curr. Biol.* **17**, R443–R449 (2007).
9. Murayama, M. & Larkum, M.E. Enhanced dendritic activity in awake rats. *Proc. Natl. Acad. Sci. USA* **106**, 20482–20486 (2009).
10. Saleem, A.B., Ayaz, A., Jeffery, K.J., Harris, K.D. & Carandini, M. Integration of visual motion and locomotion in mouse visual cortex. *Nat. Neurosci.* **16**, 1864–1869 (2013).
11. Franklin, K.B.J. & Paxinos, G. *The Mouse Brain in Stereotaxic Coordinates* (Academic Press, 2008).
12. Wang, Q. & Burkhalter, A. Area map of mouse visual cortex. *J. Comp. Neurol.* **502**, 339–357 (2007).
13. Wang, Q., Sporns, O. & Burkhalter, A. Network analysis of corticocortical connections reveals ventral and dorsal processing streams in mouse visual cortex. *J. Neurosci.* **32**, 4386–4399 (2012).
14. Whitlock, J.R., Sutherland, R.J., Witter, M.P., Moser, M.B. & Moser, E.I. Navigating from hippocampus to parietal cortex. *Proc. Natl. Acad. Sci. USA* **105**, 14755–14762 (2008).
15. Whitlock, J.R., Pfuhl, G., Dagslott, N., Moser, M.B. & Moser, E.I. Functional split between parietal and entorhinal cortices in the rat. *Neuron* **73**, 789–802 (2012).
16. Nitz, D.A. Tracking route progression in the posterior parietal cortex. *Neuron* **49**, 747–756 (2006).
17. Nitz, D.A. Spaces within spaces: rat parietal cortex neurons register position across three reference frames. *Nat. Neurosci.* **15**, 1365–1367 (2012).
18. Parron, C. & Save, E. Evidence for entorhinal and parietal cortices involvement in path integration in the rat. *Exp. Brain Res.* **159**, 349–359 (2004).
19. McNaughton, B.L., Battaglia, F.P., Jensen, O., Moser, E.I. & Moser, M.B. Path integration and the neural basis of the 'cognitive map'. *Nat. Rev. Neurosci.* **7**, 663–678 (2006).
20. Wilber, A.A., Clark, B.J., Forster, T.C., Tatsuno, M. & McNaughton, B.L. Interaction of egocentric and world-centered reference frames in the rat posterior parietal cortex. *J. Neurosci.* **34**, 5431–5446 (2014).
21. Zingg, B. *et al.* Neural networks of the mouse neocortex. *Cell* **156**, 1096–1111 (2014).
22. Nakamura, K. Auditory spatial discriminatory and mnemonic neurons in rat posterior parietal cortex. *J. Neurophysiol.* **82**, 2503–2517 (1999).
23. Wilber, A.A. *et al.* Cortical connectivity maps reveal anatomically distinct areas in the parietal cortex of the rat. *Front. Neural Circuits* **8**, 146 (2015).
24. Oh, S.W. *et al.* A mesoscale connectome of the mouse brain. *Nature* **508**, 207–214 (2014).
25. Harvey, C.D., Coen, P. & Tank, D.W. Choice-specific sequences in parietal cortex during a virtual-navigation decision task. *Nature* **484**, 62–68 (2012).
26. Dombeck, D.A., Khabbaz, A.N., Collman, F., Adelman, T.L. & Tank, D.W. Imaging large-scale neural activity with cellular resolution in awake, mobile mice. *Neuron* **56**, 43–57 (2007).
27. Foldiak, P. The 'ideal homunculus': statistical inference from neural population responses. in *Computation and Neural Systems* (eds. Eeckman, F.H. & Bower, J. M.) 55–60 (Kluwer Academic Publishers, 1993).
28. Sanger, T.D. Probability density estimation for the interpretation of neural population codes. *J. Neurophysiol.* **76**, 2790–2793 (1996).
29. Ma, W.J., Beck, J.M., Latham, P.E. & Pouget, A. Bayesian inference with probabilistic population codes. *Nat. Neurosci.* **9**, 1432–1438 (2006).
30. Ernst, M.O. & Banks, M.S. Humans integrate visual and haptic information in a statistically optimal fashion. *Nature* **415**, 429–433 (2002).
31. Körding, K.P. & Wolpert, D.M. Bayesian integration in sensorimotor learning. *Nature* **427**, 244–247 (2004).
32. Brunton, B.W., Botvinick, M.M. & Brody, C.D. Rats and humans can optimally accumulate evidence for decision-making. *Science* **340**, 95–98 (2013).
33. Jones, J.L. *et al.* Orbitofrontal cortex supports behavior and learning using inferred but not cached values. *Science* **338**, 953–956 (2012).
34. George, D. & Hawkins, J. Towards a mathematical theory of cortical micro-circuits. *PLoS Comput. Biol.* **5**, e1000532 (2009).
35. Shipp, S., Adams, R.A. & Friston, K.J. Reflections on agranular architecture: predictive coding in the motor cortex. *Trends Neurosci.* **36**, 706–716 (2013).
36. Beck, J.M. *et al.* Probabilistic population codes for Bayesian decision making. *Neuron* **60**, 1142–1152 (2008).
37. Rao, R.P.N. & Ballard, D.H. Predictive coding in the visual cortex: a functional interpretation of some extra-classical receptive-field effects. *Nat. Neurosci.* **2**, 79–87 (1999).
38. Denève, S., Duhamel, J.R. & Pouget, A. Optimal sensorimotor integration in recurrent cortical networks: a neural implementation of Kalman filters. *J. Neurosci.* **27**, 5744–5756 (2007).
39. Boccara, C.N. *et al.* Grid cells in pre- and parasubiculum. *Nat. Neurosci.* **13**, 987–994 (2010).

ONLINE METHODS

All animal procedures were conducted in accordance with guidelines of the Okinawa Institute of Science and Technology Institutional Animal Care and Use Committee in an Association for Assessment and Accreditation of Laboratory Animal Care (AAALAC International)-accredited facility. Mice were housed individually in a temperature-controlled room with 12-h/12-h light/dark cycle. All behavioral training and imaging experiments were conducted during the dark cycle.

Chronic window preparation. We used eight male C57/BL6N mice (Charles River Japan), 9–20 weeks of age. Before surgery, mice were restricted to 1.5 ml of water per day for at least 2 weeks. Mouse weight was checked daily to avoid dehydration. One day before surgery, mice got free water access. Surgery was done as described before[40] under ketamine/xylazine anesthesia (0.1 mg/g and 0.02 mg/g intraperitoneal (IP)) in a stereotaxic frame to immobilize the head. Eye ointment was applied, and carprofen (5 mg/g, IP), buprenorphine (0.1 mg/g subcutaneous), dexamethasone (2 µg/g intramuscular) and ciprofloxacin (0.02 mg/g, IP) were administered. Ciprofloxacin was also applied once per week to avoid infection after surgery.

After opening the skin, the skull was cleaned with a lidocaine solution and a craniotomy was made over the posterior parietal cortex (PPC: 1.7 mm posterior and 1.6 mm lateral of the bregma)[11,25] and secondary visual cortex (V2: 2.7 mm posterior and 1.6 mm lateral)[11] with the center at 2.2 mm posterior and 1.6 mm lateral of the bregma in the right hemisphere with a diameter of 5.5 mm, without puncturing the dura mater. PPC coordinates were the same as in a recent study[25], and the coordinates of V2 correspond to the posteromedial cortex (PM)[12,13]. We mixed AAV2/1-hSyn-GCaMP6f (2E13 GC/ml, UPenn Vector Core), AAV2/1-hSyn-TurboRFP (3E13 GC/ml, UPenn Vector Core), and PBS at a ratio of 1:1:2, and injected the mixture at two or three sites (70–100 nl in 8–15 min per site; depth 400 µm) to label PPC and PM neurons. Injections were conducted with beveled quartz pipettes with a tip opening of 7.5 to 12.5 µm using a custom air pressure injection system. A 5-mm diameter glass window (#1.5, W.P.I.) was mounted directly onto the dura and sealed with super glue. For later head restraint, a rectangular aluminum head plate with a 6 mm central opening (weight 340 mg) was positioned over the glass window and attached with dental acrylic[40]. After surgery, water was presented freely until the mouse recovered, typically for 2–3 d.

Behavioral training. After recovery from surgery, behavioral training started. Mouse weight was carefully monitored, and additional water was given after daily training to keep the weight over 85% of the pre-surgery weight. Training was conducted with head-restrained mice on a spherical treadmill[25,26]. 12 tweeter speakers around the treadmill provided auditory stimuli (speaker: FT28D, Fostex; generator: Octa-capture, Roland). Prior to experiments, speakers were calibrated with a 1/4-inch microphone (Type 4954, Brüel and Kjaer). Rotations of the spherical treadmill were measured with an optical computer USB mouse placed at the equator of the ball behind the mouse[25]. Rotation velocity parallel to the mouse's body axis was used to move forward or backward in the virtual environment indicated by tone volume and angle updated online with a median refresh rate of 62.5 Hz. The virtual environment system was controlled by custom software (LabView) with a multifunction data acquisition board (USB-6212, National Instruments).

In the auditory virtual navigation task, a virtual sound source was placed at the front left side of the mouse (**Fig. 1a**). The sound source generated a harmonic sound pulse every 80 ms with a duration of 70 ms, frequencies of 2, 4, 8, 16 and 32 kHz, and an intensity of 100 dB SPL (sound pressure level in decibels with respect to 20 µPa) at 25-cm in virtual distance. The intensity decreased by 6 dB SPL when the apparent distance between the sound source and mouse doubled. The virtual direction of the sound source was emulated by changing the sound-generating speakers according to the mouse's locomotion on the treadmill. To emulate a position between two speakers, both neighboring speakers simultaneously generated sounds with adjusted amplitudes. We employed high-intensity sounds, because a continuous broad-band background noise (70 dB SPL at the peak frequency of 7 kHz) from the air flow of the spherical treadmill reduced sound responsiveness of neurons at low intensities[41]. We verified the sound responsiveness and sound-azimuth preferences of PPC and PM neurons under the masking effect of background noise (**Supplementary Fig. 4**)[22].

A spout was placed in front of the mouse to deliver 4 µl water with 5% sucrose (2 × 2 µl water drops with an interval of 512 ms) as a reward. Sucrose water was delivered with a syringe pump (O'hara, http://www.ohara-time.co.jp/). Licking was detected by an infrared sensor with the maximum frequency of 10 Hz.

Each trial started with a harmonic tone (3, 6, 9, 18 and 36 kHz, 970 ms) that had the same intensity and direction as the tone from the sound source. After this start tone, the mouse could run in the virtual environment and when the mouse passed the sound source (i.e., goal) and licked the spout, it got the water reward. A reward tone (10 kHz, 85 dB SPL, 3 s) was presented at reward delivery to stress successful completion of a trial. When the mouse did not lick and passed the goal by 134 cm, the trial failed and an error tone was presented (1 kHz, 85 dB SPL, 1 s). The trial also failed if a mouse ran backward 50 cm from the start. The inter-trial interval (ITI) was 7 s and 9 s in reward and error trials, respectively. Each trial had a random virtual distance from the start to goal between 67 and 134 cm.

The task had three conditions designated continuous, intermittent 1 and intermittent 2. One of the conditions was randomly assigned in each trial with probabilities of 70, 15 and 15%, respectively (**Fig. 1a**). In the continuous condition, the harmonic sound was continuously presented during a trial. In intermittent conditions, sounds were intermittently presented; sound-zones and no-sound zones were alternately positioned based on distance from the goal. The center of no-sound and sound zones was placed at the goal in intermittent 1 and intermittent 2 condition, respectively. Each zone was 17 cm long. In intermittent conditions, sound was always presented 33 cm from the start, so that mice could not identify the type of trial condition at the start. Mice got the reward in 7.4 ± 0.1 s (mean ± s.e.m., n = 94). In intermittent conditions, mice spent 860 ± 10 ms (n = 94) in each no-sound zone.

On the first day of behavioral training, a mouse was placed on the treadmill and received the sucrose-water reward 100–200 times. Mice were then trained to run a short distance with tones and to lick for the reward. The running distance gradually increased trial by trial from 0 to 134 cm. After a mouse succeeded in getting the reward in the continuous condition in the auditory virtual navigation task, intermittent-condition trials were presented. Mice required three to four weeks to lick only near the goal (**Fig. 1b**). All animals tested (n = 8) were able to learn the task.

Muscimol injection. To investigate whether PPC was involved in action-dependent distance estimation, we conducted an inactivation experiment with the GABA-A receptor agonist, muscimol (Sigma). We used three male C57/BL6N mice for this experiment. Water restrictions and behavioral tasks were identical with those for mice for imaging. Also, chronic window preparation was conducted. A craniotomy was made over PPC in both hemispheres. Two access-port windows[40] were mounted directly onto the dura for bilateral injection of muscimol (1 ng/1 nl, 70 nl, diluted with PBS, 7 nl/min) into PPC with beveled quartz pipettes with a tip opening of 7.5–12.5 µm. The amount and concentration of muscimol followed a previous study of PPC inactivation in mice[25].

After training for the auditory virtual navigation task, the muscimol experiment was performed. Injections were performed under isoflurane anesthesia (2% at induction and 1% for maintenance) in a stereotaxic frame. 2 h after the injection, the behavioral task started. Every day one session was conducted, alternately either with muscimol or PBS (70 nl) injection (**Fig. 1d**). After the last session, we injected DiI to approximate the injection locations with histology. Inactivation of PPC decreased the locomotion speed of mice in the continuous condition (Mann-Whitney U-test, $P = 9.63 \times 10^{-12}$, $z = 6.81$), which was most probably caused by increased anticipatory licking (Mann-Whitney U-test, $P = 6.92 \times 10^{-11}$, $z = 6.52$). In intermittent conditions, inactivation of PPC did not change the locomotion speed ($P = 0.106$, $z = 1.62$) and the licking ($P = 0.0828$, $z = 1.73$).

We used five male C57/BL6N mice to investigate the spread of muscimol histologically. We injected fluorophore-conjugated muscimol (muscimol-BODIPY^{R} TMR-X conjugate) (1 ng/nl, 70 nl, diluted with PBS, 7 nl/min) into PPC with the same type of pipettes as for the standard muscimol injections. Muscimol-BODIPY was injected in the left, the right, or both hemispheres of PPC (1 left, 2 right, 2 both). Muscimol-BODIPY spreads approximately half or one-third compared to the standard muscimol[42,43]. In this study, spread of muscimol-BODIPY was about 150 µm in radius (**Supplementary Fig. 2a**). As the deep cerebral white matter works as a diffusion barrier[42,44], the spread of muscimol was mainly in PPC.

Imaging. After training of the auditory virtual navigation task, 3–4 weeks after viral injections, imaging experiments were started. Imaging was conducted for 3–4 weeks, but no longer than 7 weeks after AAV injection. Additionally, when we observed bright cells with GCaMP6f that did not show calcium signals, we stopped collecting data from the mouse in question. We selected 1–3 locations in each mouse and imaged at different depths from layers 2, 3 and 5, such that recordings were acquired from the same column in different layers. We imaged 2–21 planes per mouse. On each experimental day, we imaged one plane of one location.

Imaging was performed using a custom-built two-photon microscope (MOM, Sutter Instrument) with either a 5×/N.A. 0.25 air objective (Zeiss) or a 25×/N.A. 1.05 water immersion objective (Olympus). The 5× objective was used to image the blood vessel pattern of the cortical surface (**Fig. 2a**), while the 25× objective was used to image cortical layers 2, 3 and 5 at cellular resolution during the task.

An ultrafast Ti:sapphire laser (Vision II, Coherent) was operated at 950 nm to excite fluorescence, which was detected with two GaAsP photomultiplier tubes (Hamamatsu) in the spectral range of 490–560 nm (green) and 570–640 nm (red) separated by a 565-nm dichroic mirror (all Chroma). A resonant scanning system was used to acquire images at 30.9 Hz at a resolution of 512 × 512 pixels corresponding to a 400 × 400 μm^2 field of view with the 25× objective. The microscope and image acquisition were controlled by commercial software (MScan, Sutter Instrument). Timing of image acquisition, i.e. the command signals of the scanners, the sound presentations, the water presentations, the on-off of infrared sensor for licking, and updates of the virtual environment were recorded simultaneously with a sampling rate of 500 Hz (PCI-6225, National Instruments) controlled by custom-designed software written in LabView (National Instruments). In each session, we imaged for about one hour continuously up to 120,000 frames in more than 150 trials of the task. Slow drifts of the imaging plane were rarely observed. However, if drift occurred, the objective position was manually adjusted (typically 1 µm) during the inter-trial interval to retain the recording site as precisely as possible.

Histology. After imaging experiments, mice were deeply anesthetized with ketamine/xylazine (0.1 mg/g and 0.02 mg/g, IP) and transcardially perfused with 4% paraformaldehyde, 0.2% sodium meta-periodate and 1.4% lysine in PBS. The brain was carefully removed from the cranial bone. After checking the fluorescent area in the whole brain, sections were cut at 100 µm with a vibratome (VT1000S, Leica), mounted, and imaged with a wide-field fluorescence microscope (M165FC, Leica) and photographed with an SLR camera (Nikon). Imaging locations were determined based on the blood-vessel pattern, the relative position of the fluorescent area and subcortical structures[11].

Data analysis. All analyses were conducted with ImageJ (US National Institutes of Health) and Matlab (MathWorks) with a desktop computer (6-core 3.06 GHz Intel Xeon X5675) or a high performance computing (HPC) cluster (12-core 2.50 GHz Intel Xeon E5-2680v3). In the figures, error bars represent s.e.m. Error bars of the median represent robust standard error (1.4826×MAD/sqrt(n); MAD = median absolute deviation; n = number of data points)[45].

Behavioral analysis. In every behavioral task session (one per day, one imaging plane at one location), we analyzed the first 150 trials. Trials in which mice took more than 20 s to get a reward, were excluded from analyses (2.71% of trials per session), as were error trials (0.142%). To check whether mice listened to the sound during the task, we analyzed the initiation of licking. If mice licked only near the goal (**Fig. 1b**), the start-to-lick distance correlated with the start-to-goal distance. Only sessions with a significantly positive correlation were used for analyses ($P < 0.01$), and sessions with no significant correlations were discarded (4 sessions of 100). Initiation of licking was defined as the first lick more than 33 cm from start, so that licks around the start were not included. In total, we analyzed data from 94 sessions in 8 mice (mouse 1, 2 sessions; mouse 2, 10 sessions; mouse 3, 5 sessions; mouse 4, 14 sessions; mouse 5, 15 sessions; mouse 6, 15 sessions; mouse 7, 12 sessions; mouse 8, 21 sessions).

Neural analysis. Although we observed almost no motion artifacts in the recorded images, we conducted a simple motion correction. We calculated the averaged image of all red-channel frames in one session, and each red-channel frame was shifted in X-Y axes to minimize differences of pixel intensities between the frame and averaged image. The maximum correction was ten pixels (8 µm) and sessions in which the motion correction was apparently not enough were not used in analyses (2 sessions of 100). Regions-of-interest (ROIs) for putative cells were then selected manually. Signals of each cell were defined as the averaged pixel values inside an ROI, and were measured as ratio of the green/red channel to minimize the effect of motion artifacts.

Among manually selected ROIs, we defined active ROIs as containing a signal beyond 3σ during a session. If ROIs did not show any signals, they were discarded (0.399%) (**Supplementary Table 1**). A portion of these neurons may have over-expressed GCaMP6f. We used the ratio of green and red channel intensities $R(t)$ to calculate $\frac{\Delta R}{R}(t)$ of each active ROI:

$$\frac{\Delta R}{R}(t) = \frac{R(t) - \mathrm{mean}(R)}{\mathrm{mean}(R)} \quad (1)$$

where $mean(R)$ is the averaged intensity ratio $R(t)$ of all 150 trials including inter trial intervals.

Task-relevant neurons. For every neuron, all trial traces $\frac{\Delta R}{R}(t)$ were aligned at the following marks: (i) temporally with the trial start indicated by the start tone, (ii) temporally with reaching the goal, (iii) temporally with the first lick, (iv) spatially with respect to the start position, and (v) spatially with respect to the goal distance. Neural activities of each neuron were averaged and then moving averaged with 500 ms for time-aligned activities or moving averaged with 8.37 cm with a step size of 0.42 cm for distance-aligned activities. We defined a neuron as task relevant when the aligned and averaged activity had a significantly positive value at any time point or distance point compared to baseline (one-sided one-sample t test, $P < 10^{-10}$). When neurons showed a significant start-aligned activity within two seconds of the trial start ((i) or (iv)), we defined them as start neurons. When neurons showed significant goal-aligned activity ((ii) or (v)), we defined them as goal-distance neurons or reward neurons, as described hereafter. We also detected neurons that showed significant activity during the onset of licking behavior, which we denominated lick neurons (iii).

Among neurons with significant goal-aligned activity, we first determined each neuron's time point of peak activity. We then grouped neurons as before-reaching or after-reaching, dependent on whether the time point of peak activity occurred before or after reaching the goal. Further, for after-reaching neurons, we analyzed neural activity of the last 500 ms (16 frames) before reaching the goal and categorized neurons into two groups with k-means clustering. After-reaching neurons started to increase activity before the goal (ramping activity), while reward neurons increased their activity only after reaching it (**Fig. 2d**). We defined before-reaching and after-reaching neurons as goal-distance neurons.

Some neurons showed significant activity under several alignments so that they could be categorized into several types. First, we categorized neurons as start-neurons, goal-distance neurons, or both, because the distance between start and goal was randomly assigned in each trial; therefore, the activity added up or averaged out depending on the alignment. In contrast, the timing of goal-reaching and first-lick were correlated. We assigned a neuron as either a goal-distance or a lick neuron, depending on whether the higher significance occurred during goal-aligned or lick-aligned activity.

Regression analysis. To further investigate task-relevant neurons, especially goal-distance neurons, we conducted a regression analysis to test whether neurons represented the time or distance to reach the goal. We also investigated whether neurons represented licking frequency or locomotion speed. The regression analysis was defined as

$$\begin{cases} y(t) = \beta_0 + \beta_1\varphi_1(\mathrm{distance}(t)) + \beta_2\varphi_2(\mathrm{lick}(t)) + \beta_3\varphi_3(\mathrm{speed}(t)) \\ y(t) = \beta_0 + \beta_1\varphi_1(\mathrm{time}(t)) + \beta_2\varphi_2(\mathrm{lick}(t)) + \beta_3\varphi_3(\mathrm{speed}(t)) \end{cases} \quad (2)$$

where $\beta_{0\text{-}3}$ are regression coefficients, and $y(t)$ is the unfiltered neural activity trace $\frac{\Delta R}{R}(t)$. distance(t), time(t), lick(t) and speed(t) are goal distance, goal time, licking frequency and locomotion speed at frame t, respectively. φ_i is the Gaussian basis function:

$$\varphi_i(x) = \exp\left\{-\frac{(x-\mu_i)^2}{2s_i^2}\right\} \quad (3)$$

doi:10.1038/nn.4390

where s_i is a free parameter that determined how sharply a neuron represented each variable. μ_i was pre-determined and was either the distance, time, licking frequency or locomotion speed at maximal averaged neural activity. For every neuron, the data from all 150 trials were used in the regression analysis to fit β_{0-3} and s_{1-3}. We tested four different initial values for each s to avoid local minima. Our regression analysis used a Gaussian function, instead of the usually used linear function, because PPC neurons are known to have place-specific activity[25]. In equation (2), we tested all possible combinations of variables (11 combinations: distance, distance/lick, distance/speed, distance/lick/speed, time, time/lick, time/speed, time/lick/speed, lick, speed, lick/speed). The best fitting variables were determined with the Bayesian information criteria (BIC) based on the sum of squared errors in the regression analysis[46,47]

$$BIC = N\log\left[\frac{1}{N}\sum_{t=1}^{N}\{y(t)-\hat{y}(t)\}^2\right] + k\log(N) \quad (4)$$

where $\hat{y}(t)$ was the output of equation (2) with fitted parameters (β_{0-3} and s_{1-3}), N was the number of total frames during all 150 trials, and k was the number of parameters.

We conducted a linear regression analysis to investigate whether the activity of after-reaching neurons increased during sound and no-sound zones. The regression analysis was defined as follows:

$$y(\text{distance}) = \beta_0 - \beta_1\,\text{distance} \quad (5)$$

where β_{0-1} were regression coefficients. y(distance) was the neural activity trace $\Delta R/R$ at a given goal distance binned every 0.42 cm. When β_1 was significantly positive ($P<0.05$ in a two-sided Student t test), the activity had a positive slope. Regression analysis was independently applied to the activity during each sound and no-sound zone.

Probabilistic decoding of goal distance. We employed a probabilistic decoder to analyze how precisely population activity of PPC and PM predicted goal distance. A similar decoder was used to estimate the location from hippocampal cell activity and to model Bayesian computation in the brain with probabilistic population code[29,48]. The decoder estimated goal distance from the population activity of all goal-distance neurons in one session (n = 0–175, sessions with 0 goal-distance neurons (3 sessions of 94) were excluded) as follows:

$$P(x\,|\,n_{all,t}) = \frac{P(n_{all,t}\,|\,x)P(x)}{\sum_x P(n_{all,t}\,|\,x)P(x)} \propto P(n_{all,t}\,|\,x)P(x) \quad (6)$$

where

$$P(n_{all,t}\,|\,x) = \prod_{i=1}^{all} P(n_{i,t}\,|\,x) \quad (7)$$

x was the goal distance and $n_{i,t}$ was the $\frac{\Delta R}{R}$ value of the i-th neuron at frame t after a moving average with a bin-width of 3 frames (97.1 ms). The decoder assumed that the activity of each neuron was independent.

For calculating the likelihood of the decoder $P(n_{all,t}\,|\,x)$, we first calculated a distance tuning curve for every goal-distance neuron from all trials under the continuous condition (n = 105 trials per session on average). The goal distance was split into 4.2-cm bins. Then the mean $\mu_{i,x}$ and s.d. $\sigma_{i,x}$ of logarithmic neural activity were analyzed in each bin with a maximum likelihood estimate (Matlab). Means and s.d. were smoothed with a Gaussian kernel with a s.d. of 4.2 cm, and they were re-sampled every 0.84 cm. Activity traces were individually shifted parallel for every neuron such that all $n_{i,t}$ became positive for the likelihood estimation with a log-normal distribution:

$$P(n_{i,t}\,|\,x) = \frac{1}{n_{i,t}\sigma_{i,x}\sqrt{2\pi}}\exp\left[-\frac{\{\ln(n_{i,t})-\mu_{i,x}\}^2}{2\sigma_{i,x}^2}\right] \quad (8)$$

The decoder with log-normal distribution gave better estimates for goal distance than that with a Gaussian distribution in the 18 settings (estimates in layers 2, 3 and 5 of PPC and PM in both continuous and intermittent conditions) (Wilcoxon signed rank test, P = 0.00609 to 0, z = 2.74 to 31.9), except for layer 5 in PM in continuous condition (P = 0.834, z = 0.209). It also performed better than a decoder with gamma distribution (P = 0.00189 to 0, z = 3.11 to 27.6) except for five settings (that is, layer 2, 3 of PPC and layer 3, 5 of PM in intermittent 1 condition and layer 2 of PPC in intermittent 2 condition (P = 0.230 to 0, z = 1.20 to 10.6)). We used a flat prior of the decoder $P(x)$ (that is, non-informative prior) to clearly test the decoding performance of neurons.

In the continuous condition, we employed a leave-one-out cross validation for evaluating decoding performance[46]. For cross validation, one trial of continuous-condition data was used for validation, while the rest of the data were used for training. Training data were used to build the decoder by determining the tuning curves of all goal-distance neurons for likelihood estimation. The decoder then estimated the goal distance from the neural activity of validation data and compared it with the actual distance. We tested all combinations of validation and training data to estimate the distances in all trials.

In intermittent 1 and intermittent 2 conditions, the continuous-condition data was used for training the decoder. The decoder then estimated goal distances in intermittent conditions. This procedure enabled us to test whether distance predictions during no-sound zones were equivalent to those with continuous sound cues.

As the probabilistic decoder provided distributions of predictions, we focused on its root mean squared error, mode (maximum a posterior: MAP) and s.d. from mode (uncertainty) (**Fig. 4**). The root mean squared error (RMSE) is defined as

$$\text{RMSE}(t) = \sqrt{\sum_x P(x\,|\,n_{\text{all},t})(x-\hat{x}(t))^2} \quad (9)$$

where $\hat{x}(t)$ was the position of mouse at frame t.

To investigate how MAP and uncertainty changed during sound and no-sound zones, we conducted a linear regression analysis:

$$y(t) = \beta_0 - \beta_1\,\text{distance}(t) \quad (10)$$

where $y(t)$ was either MAP or uncertainty of posterior distribution at frame t. Regression analysis was independently applied to each sound and no-sound zone in single trials.

Our probabilistic decoder assumed that activity of each neuron was independent. To assess the effect of neural correlations, we used a support vector machine (SVM) (Matlab) and compared the performances between SVM trained with recorded data (recorded-SVM) and SVM with shuffled data (shuffled-SVM)[49,50]. Recorded-SVM and shuffled-SVM did and did not take into account neural correlations. The two decoders were trained and validated in the same manner as the probabilistic decoder. Recorded-SVM did not estimate distance better than shuffled-SVM (one-sided Wilcoxon signed-rank test, P = 0.957 to 1, z = 1.71 to 12.5), except in 1 setting (layer 3 in PM in intermittent1 condition, P = 0.00572, z = 2.53), which justifies the assumption of independence in probabilistic decoding. The reason for this might be the larger amount of data required for a decoder to take into account correlated neural activities, or it could also be the low temporal resolution of calcium activity.

Imaging sound responses of neurons. Prior to every imaging experiment of the auditory virtual navigation task, we investigated the sound responsiveness of neurons in the field of view. We presented the harmonic sound of the task (2, 4, 8, 16 and 32 kHz, 100 dB SPL, 200 ms) from every one of the 12 speakers separately. Inter-stimulus interval was 5 s. The order of sound presentations was pseudo-random. Each speaker presented the sound ten times so that the total number of sound presentations was 120.

Analysis of sound responses of neurons. We analyzed whether PPC and PM neurons responded to sound. Neural activity following sound presentation from two adjacent speakers was analyzed together. Activity was tested for sound azimuths of 0, π/3, 2π/3, π, 4π/3, 5π/3 degrees (**Supplementary Fig. 4**). Activity was moving averaged over 500 ms, and when activity within the first 1.5 s of the sound presentation was significantly larger than spontaneous activity during 1 s before sound presentation (one-sided Student's t test, $P < 10^{-5}$), we defined the neuron as sound responsive. Here the significance threshold was weaker than that for the task ($P < 10^{-10}$), because there were fewer data points. Among sound-responsive neurons, we tested the azimuth at which each neuron showed maximum activity. Latency was defined as the time between tone onset and when activity first reached the significance threshold at the preferred azimuth ($P < 10^{-5}$).

Statistics. Task-relevant neurons were defined based on one-sample *t*-test. In other comparisons, we conducted a normality test (Lilliefors test, Matlab) and decided to use non-parametric tests. We mainly used two-sided Mann-Whitney *U*-test, Wilcoxon signed rank test or Ansari-Bradley test. Clear statement was added in one-sided test. Variances of data were compared in **Fig. 1e**, but variances were not statistically tested in the other data. In multiple comparisons (**Figs. 1c**,**f**, and **2d**), we set the significant threshold as $P < 0.01$ to meet Bonferroni correction. In 4 of 8 mice, we imaged neuronal activity in both PPC and PM. Sessions for imaging PPC and PM were switched every 3–7 sessions. Order of PPC and PM sessions had no significant difference (Mann-Whitney *U* test, $P = 0.755$, $z = 0.312$). Data collection and analysis were not performed blind to the conditions of the experiments. No statistical methods were used to pre-determine sample sizes but our sample sizes are similar to those generally employed in the field.

A **Supplementary Methods Checklist** is available.

Code availability. Data analyses were conducted in Matlab scripts which are available from corresponding author upon request.

Data availability. The data that support the findings of this study are available in https://groups.oist.jp/ncu/data.

40. Roome, C.J. & Kuhn, B. Chronic cranial window with access port for repeated cellular manipulations, drug application and electrophysiology. *Front. Cell. Neurosci.* **8**, 379 (2014).
41. Phillips, D.P. & Cynader, M.S. Some neural mechanisms in the cat's auditory cortex underlying sensitivity to combined tone and wide-spectrum noise stimuli. *Hear. Res.* **18**, 87–102 (1985).
42. Allen, T.A. *et al*. Imaging the spread of reversible brain inactivations using fluorescent muscimol. *J. Neurosci. Methods* **171**, 30–38 (2008).
43. Martin, J.H. Autoradiographic estimation of the extent of reversible inactivation produced by microinjection of lidocaine and muscimol in the rat. *Neurosci. Lett.* **127**, 160–164 (1991).
44. Erlich, J.C., Brunton, B.W., Duan, C.A., Hanks, T.D. & Brody, C.D. Distinct effects of prefrontal and parietal cortex inactivations on an accumulation of evidence task in the rat. *Elife* http://dx.doi.org/10.7554/eLife.05457 (2015).
45. Adesnik, H., Bruns, W., Taniguchi, H., Huang, Z.J. & Scanziani, M. A neural circuit for spatial summation in visual cortex. *Nature* **490**, 226–231 (2012).
46. Bishop, C.M. *Pattern Recognition and Machine Learning*, Vol. 1 (Springer, 2006).
47. Ito, M. & Doya, K. Distinct neural representation in the dorsolateral, dorsomedial, and ventral parts of the striatum during fixed- and free-choice tasks. *J. Neurosci.* **35**, 3499–3514 (2015).
48. Pfeiffer, B.E. & Foster, D.J. Hippocampal place-cell sequences depict future paths to remembered goals. *Nature* **497**, 74–79 (2013).
49. Averbeck, B.B., Latham, P.E. & Pouget, A. Neural correlations, population coding and computation. *Nat. Rev. Neurosci.* **7**, 358–366 (2006).
50. Graf, A.B., Kohn, A., Jazayeri, M. & Movshon, J.A. Decoding the activity of neuronal populations in macaque primary visual cortex. *Nat. Neurosci.* **14**, 239–245 (2011).